International Journal of
INTELLIGENT SYSTEMS AND APPLICATIONS IN ENGINEERING

IJISAE

ISSN:2147-6799 www.ijisae.org Original Research Paper

Mayenite Electride and Nanostructured Magnetite Composites for Microwave Absorption

Dr. Anamika Singh[1], Sunit Sizariya[2]

Submitted: 08/10/2023 **Revised:** 16/11/2023 **Accepted:** 02/12/2023

Abstract: The electronic and communication industries are rapidly growing in order to satisfy the demands of contemporary society, thanks to the emergence of 5G technologies including IoT. In this situation, improved microwave attenuating substances are necessary to protect electronics, communication equipment, and biological systems. This paper talks about some important attempts to create advanced materials that may effectively reduce microwave signals. The stable inorganic electride C12A7:e- with modified graphene interfaces (C12A7:e-/MG) offers a high-frequency EM response suitable for effective microwave absorption in the 5G bands. The structure and morphology-derived microwave absorption properties of C12A7:e- can be further improved by modifying the nature of carbon interfaces as it can offer better interfacial polarization and electrical conductivity. Among the class of ferrites, Magnetite has instilled a great interest in material scientists due to its excellent biocompatibility, easy control over size and morphology, and better thermal properties. This study investigates the high-frequency microwave absorption properties of C12A7:e- with highly graphitized carbon interfaces (C12A7:e-@G) and C12A7:e-@G incorporated with Magnetite nanoparticles (NPs) having different sizes and morphology.

Keywords: *electronic and communication, 5G technologies, microwave attenuating substances, microwave signals, inorganic electride, modified graphene interfaces, EM response, high-frequency microwave absorption properties, Magnetite nanoparticles*

Introduction

The immense development in the application of high-frequency EM radiation for electronic and communication systems demands high-frequency microwave absorbers. The stable inorganic electride C12A7:e- with modified graphene interfaces (C12A7:e-/MG) offers a high-frequency EM response suitable for effective microwave absorption in the 5G bands. The structure and morphology-derived microwave absorption properties of C12A7:e- can be further improved by modifying the nature of carbon interfaces as it can offer better interfacial polarization and electrical conductivity. However, the increased conductivity results in poor impedance matching and can be compensated by incorporating magnetic materials. The magnetic part in the composite material can also enhance the microwave absorption by various magnetic losses and the polarization at the interfaces of different species in the composites (Jiao et al., 2020; Lv et al., 2017).

[1]*Assistant Professor, School of Computer Science and Technology, LNCT University, Bhopal (M.P.), India*

[2]*Research Scholar, School of Computer Science and Technology, LNCT University, Bhopal (M.P.), India*

The magnetic losses come from different resonance mechanisms such as domain wall resonance, natural resonance, exchange resonance, and eddy current loss. Domain wall resonance occurs at lower frequencies, and hence other resonance mechanisms are possible in microwave frequencies (Shukla, 2019). High-frequency stability of permeability is one of the criteria which needs to be satisfied by material to act as the magnetic counterpart in a microwave absorbing system. Snoek's limit suggests that this condition is fulfilled by magnetic materials having high saturation magnetization (Ms). In spite of the fact that magnetic metals like iron, cobalt, and nickel, as well as their alloys, are capable of meeting this criterion, the high conductivity of these materials results in a reduction in permeability due to the elevated eddy current loss. As a result of its reduced Ms and Eddy current loss, ferrites have gained widespread acceptance as a potential replacement for magnetic metals. According to Liang et al.'s research from 2020, the magnetic characteristics of ferrites can be modified by altering the size and morphology of the material. This is because the size and morphology have a major influence on the surface area, anisotropy, and resonance frequency.

Among the class of ferrites, Magnetite has instilled a great interest in material scientists due to its excellent biocompatibility, easy control over size and morphology, and better thermal properties. Several studies have been reported based on the microwave absorption properties of Magnetite based composite materials, usually integrated with graphene, carbon nanotubes, semiconductors, metal-organic framework (MOF) derived structures, MXenes, etc. This study investigates the high-frequency microwave absorption properties of C12A7:e- with highly graphitized carbon interfaces (C12A7:e-@G) and C12A7:e-@G incorporated with Magnetite nanoparticles (NPs) having different sizes and morphology.

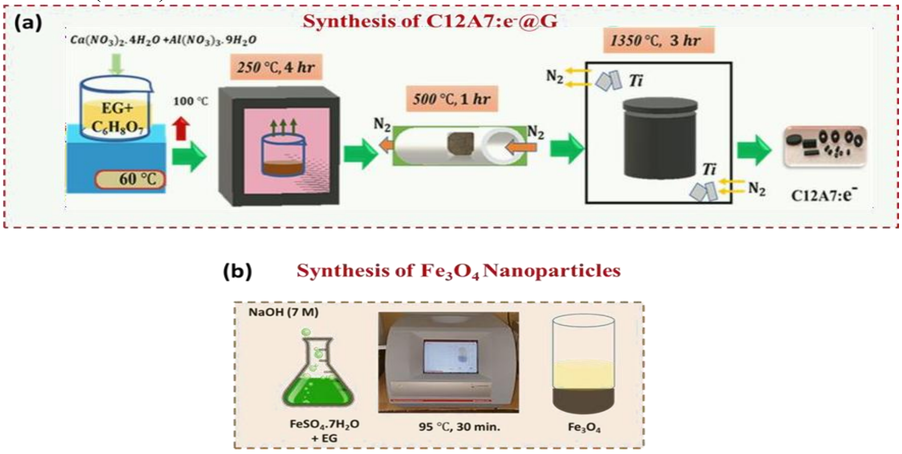

Fig. 1 (a) Sol-gel synthesis of C12A7:e-@G and (b) microwave synthesis of Magnetite

Literature Review

Due to the remarkable progress made in telecommunications technology, older devices are being replaced by more complex and integrated devices. This, in turn, has resulted in an increased demand for superior EMI shielding and MAMs. Hunt for advanced functional electromagnetic interference shielding as well as microwave attenuating substances for a variety of uses is clearly evident in the research sector. Figure 2 (a) illustrates the number of articles on EMI shielding along with MAM between 2000 and 2022 (Scopus data collected using the keywords "EMI shielding" and "Microwave absorbing materials"). The pie chart in Fig 2 (b) along with (c) shows percentage of articles for each year. The significant increase in number of research articles every year demonstrates the growing impact of EMI and the current demand for more advanced EMI shielding materials. The most effective method for shielding a device from undesirable electromagnetic interference is to cover it with a protective substance. The present work on EMI- shielding substances mostly concentrates on the selection of materials, production strategies, domains of application, and multifunctionality. In addition, it takes into account the cost-effectiveness of the shielding substance as well as its compatibility with the environment. The advancements in EMI shielding materials begin with metallic shields and continue with the creation of new, improved functional materials.

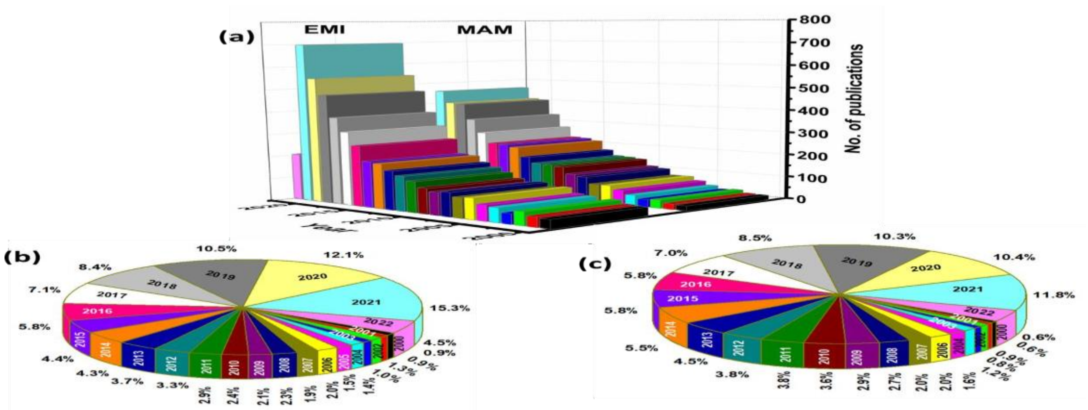

Fig. 2 (a) The number of articles on EMI shielding and MAM, (b) a pie chart displaying the proportion of articles on EMI shielding, and (c) a pie chart indicating the percentage of publications on MAM throughout the period between 2000 and 2022

Electrides generally are a relatively newer kinds of ionic solids. In these substances, electrons that are stuck in a chemical cavity are considered to be the smallest anions. Cavity-trapped electron is found in the same places as anions in ionic solids. It is neither localised on individual atoms or molecules, nor is it delocalised like electrons in metals. First electride synthesis was accomplished by solvating electrons of any alkali metal along with complexing metal cation with crown ethers and cryptands (Ellaboudy et al., 2002). This form of organic electride is unstable even at room temperature and will break down when it comes into contact with air and moisture. Mayenite electride, that is the reducing kind of mayenite (Khan et al., 2019), is initial inorganic electride that is stable at ambient temperature. In this electride, cage-trapped electrons along with counter cations occupy separate locations. Mayenite constitutes one of the transitional stages of the CaO-Al2O3 structure, that has an equilibrium of Ca12Al14O33. For many years, it has been recognized as an important component of calcium aluminate cement, which has the formula 12CaO·7Al2O3 (C12A7) in cement-chemist notation. It is widely used for structural material applications. It comprises a cube group of I-43d, containing 12 cages with two formulae units in every single cell. It has a structure that resembles zeolite, with a positively charge cage structure, [Ca24Al28O64]4+, that is around 5 Å in size (Salasin et al., 2017). Two of C12A7 single-cell frames were joined using O2- ions, and those are commonly referred to simply as "extra structures" since they are not closely linked to the cages. The mass flow that happens between the inner cages and the exterior is regulated by the tiny "cage opening" of 0.1 nm (Matsuishi et al., 2003). C12A7 has a unique ability to selectively incorporate anions including OH–, O-, F–, O2-, S2–, Cl– as well as electrons as substitutes for O2−. This is an intriguing property because these anions are not typically found in traditional ceramic oxides (Dong et al., 2013). Mayenite electride C12A7:e- is the name given to mayenite in which all of the clathrate O2− ions from crystallographic cages have been replaced by electrons. These electrons create a singlet bipolaron or diamagnetic pair (Matsuishi et al., 2003) by coupling with each other antiferromagnetically. C12A7:e- has a lower work function that is similar to that of alkali metals, but it has a unique chemical and thermal stability because of its remarkable three-dimensionally connected positively charged sub-nanometre-sized cage arrangement (Toda et al., 2007). The electrons that are trapped in the cage can move throughout the crystal by jumping to nearby cages, which gives the material high conductivity.

C12A7:e- has a number of applications due to its excellent electrical conductivity. These applications include activation alongside splitting of CO_2 (Kim et al., 2006), wires circuit alongside electrodes (Hayashi et al., 2002), cathode material in fluorescent lamps (Watanabe et al., 2011), electron-injection layer in OLEDs (Yanagi et al., 2009), as well as electron emitter (secondary) in a display panel (plasma) (Ono-Kuwahara et al., 2006). EMI shielding is one of areas where the qualities of ceramic (inherently conducting), C12A7:e-, could be quite useful. However, it has not been researched yet.

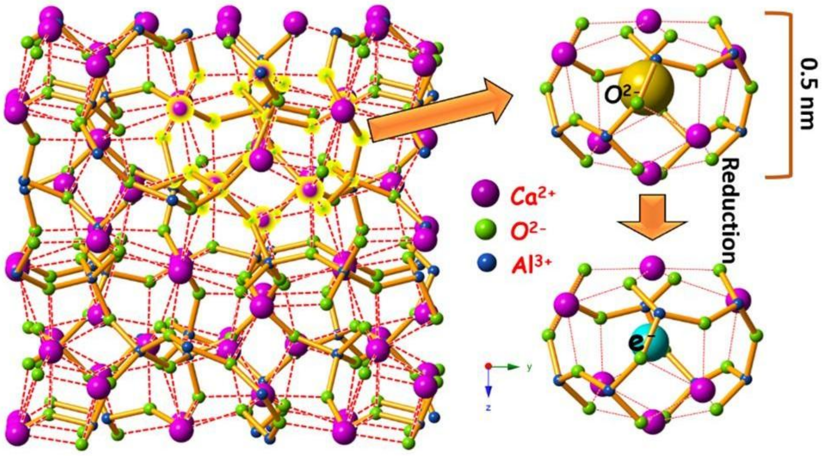

Fig. 3 The chemical makeup of C12A7 and the process of replacing cage-trapped O2- ions with electrons undergoing reduction

Along with electrical conductivity, the creation of interfaces and porosity in materials effectively brings together a number of dissipation processes (Ma et al., 2021). Although the porosity of a material might decrease its electrical conductivity, porous substances may have additional methods of internal reflections including consequent absorption of EM radiations. Furthermore, many interfaces may generate interfacial polarization, which may further degrade electromagnetic signals and enhance microwave absorption. According to Khan et al. (2019), the molecule C12A7:e- can be made more structurally and electrically stable by applying a covering of reduced graphene oxide (rGO). As a result, this study generates and examines porosity-induced C12A7:e- with graphene interfaces for the purpose of high-frequency microwave absorption and shielding. Impedance matching, which is the most important factor for microwave absorption, is examined at higher frequencies.

Experimentation

Materials

Both $Ca(NO_3)_2.4H_2O$ (with a purity of at least 99.0%) and $Al(NO_3)_3.9H_2O$ (with a purity of 98.0-102.0%) were obtained from Sigma Aldrich, Japan, and Alfa Aesar, USA, respectively. The following substances were acquired from Merck life science private limited in Mumbai: ethylene glycol (EG, $C_2H_6O_2$, 99.0%), citric acid ($C_6H_8O_7$, 99.0-102.0%), iron sulfate heptahydrate ($FeSO_4.7H_2O$), and sodium hydroxide (NaOH). A purchase of spherical magnetite nanoparticles with a particle size ranging from 50 to 100 nanometres (97%) was made from Sigma-Aldrich Company in the United States. All of the compounds were utilized in their original state, without any additional purification.

Characterization Techniques

Using a PerkinElmer STA 800 TG-DTA/DSC analyser, the thermal reactions that occurred during the synthesis of C12A7:e-@G were examined.

For the purpose of analyzing the crystal structure and phases of the materials, X-ray diffraction (XRD) was performed using a Bruker D8 Advance diffractometer. The radiation used was Cu Kα radiation with a wavelength of 1.5406 Å, 40 kV, and 40 mA. Spectra of the ultraviolet and visible spectrum were captured with a Jasco V-750 spectrophotometer. The Raman spectra were captured using a LabRAM HR evolution spectrometer that was equipped with a DPSS laser source and had an excitation wavelength of 531 nm. Microscopy techniques such as field emission scanning electron microscopy (FESEM) with an FEI-Novanano SEM 455 (10 kV beam potential) and high-resolution transmission electron microscopy (HRTEM) with an FEI Tecnai G2, F30 (300 kV accelerating potential) were utilized in order to investigate the morphology of the material.

In order to determine the amount of carbon present in C12A7:e-@G, a CHNS/O analyser from the PerkinElmer 2400 series II was utilized. Utilizing a two-probe approach and a Keithley 2400 source meter, the DC-electrical conductivity of the pellet was measured at room temperature during the measurement process. In order to conduct the surface elemental analysis, a Thermo Scientific ESCALAB X-ray Photoelectron Spectrometer (Al Kα 1486.6 eV) was utilized. A vibrating sample magnetometer (VSM) was utilized in the physical property measurement system developed by Quantum Design in the United States of America in order to record the M-H responses of magnetite nanoparticles at ambient temperature. Studies on microwave absorption in the frequency range of 5-40 GHz were conducted with a coaxial airline of 2.4 millimetres in diameter (Φin = 1.04 mm and Φout = 2.4 mm).

Results & Discussion

The minimum reflection losses (RL) achieved by the material are -22.9, -27.1, and -43.8 dB at 30.98 25.3, 19.0 GHz. The microwave attenuation of the material can be further improved by increasing its electrical conductivity and modifying the interfaces. Here, this has been achieved by simply modifying the synthesis condition. This synthesis method resulted in providing a uniform coating of highly graphitized carbon over C12A7:e- which in turn led to an improved electrical conductivity.

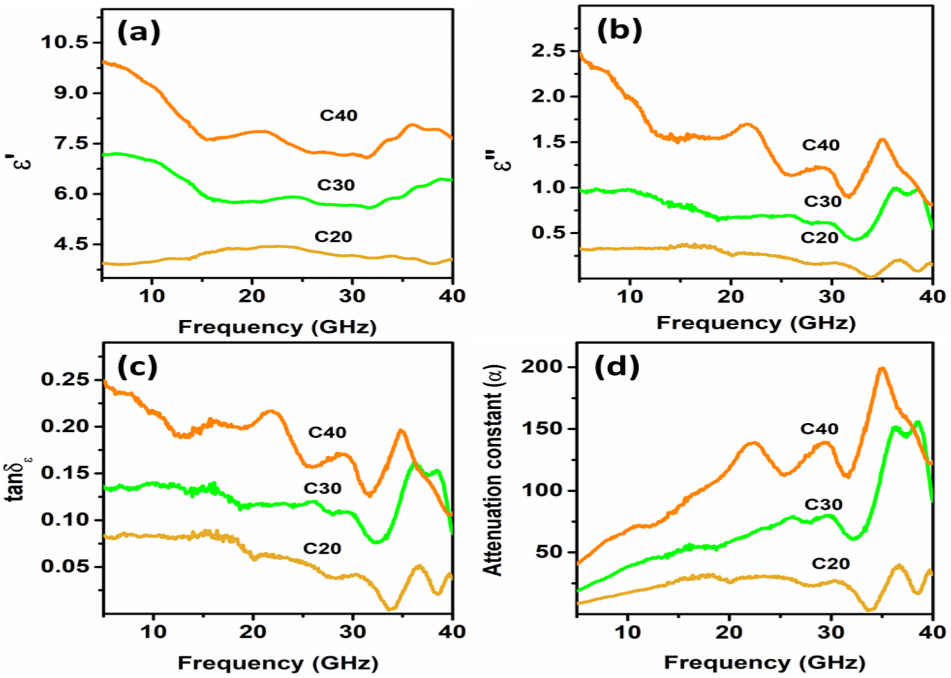

Fig. 5.11 (a) real and (b) imaginary permittivity, (c) dielectric loss tangent and (d) attenuation constant of C20, C30 and C40 composites.

Here, the microwave absorbing properties of C12A7:e-@G and Magnetite incorporated C12A7:e-@G composites are characterized in a wide frequency range from 5 to 40 GHz. Fig. 5.10 shows the RL variation of C12A7:e-@G loaded paraffin wax composite with different filler loading of 20, 30, and 40 wt% (sample codes are C20, C30, and C40, respectively). The frequency and thickness-dependent variation of RL is studied for all composites, and the corresponding 3D and 2D contours are shown in Fig. 5.10. The composites exhibit multi-band microwave absorption at higher thicknesses. C12A7:e-@G also exhibits high-frequency microwave absorption similar to C12A7:e-/MG discussed earlier. For a 2.5 mm thick C20 composite, the minimum RL is -38.2 dB at 27.7 GHz frequency. It shifts to -22.8 dB at 21.4 GHz when the thickness is further increased to 3.0 mm. The minimum RL shows an increase with the increase in C12A7:e-@G loading. For C30 and C40 composites having thickness 2.5 mm, the minimum RL are -27.2 dB and -15.4 dB resulting at frequencies 23.1 and 19.8 GHz frequencies, respectively. Also, for a thickness of 3.0 mm, the minimum RL are -18.8 and -14.6 dB at 18.5 and 16.8 GHz for C30 and C40, respectively. The increase in the RL with C12A7:e-@G indicates the poor impedance matching resulted due to the increase in electrical conductivity of the composites (Shukla, 2019). Even though higher conductivity resulted in poor impedance matching, it is an essential requirement to achieve better microwave attenuation. The variation in the microwave absorption among the composites can be better understood by the electromagnetic parameter analysis.

Fig. 4 shows the real (ε') and imaginary (ε") permittivity, dielectric loss tangent, and attenuation constants (α) of the C20, C30, and C40 composites. The complex permittivity, loss tangent, and attenuation constant shows an increase with an increase in C12A7:e-@G concentration. This indicates the increase in electrical conductivity of the composite with the increase in the concentration of the conducting filler. The poor impedance matching observed for C30 and C40 composites compared to C20 can be attributed to this increase in permittivity due to the increased electrical conductivity. However, the high attenuation constant of the composites suggests that the composites are suitable for microwave absorption applications in the high-frequency region of the microwave spectrum. The main mechanisms responsible for the microwave absorption properties of C20, C30, and C40 composites originates from the electrical conduction losses due to the high electrical conductivity of the C12A7:e- and graphitic carbon interface and interfacial polarization losses resulting from the Maxwell-Wagner-Sillar (MWS) effect at the C12A7:e- and graphitic carbon interfaces.

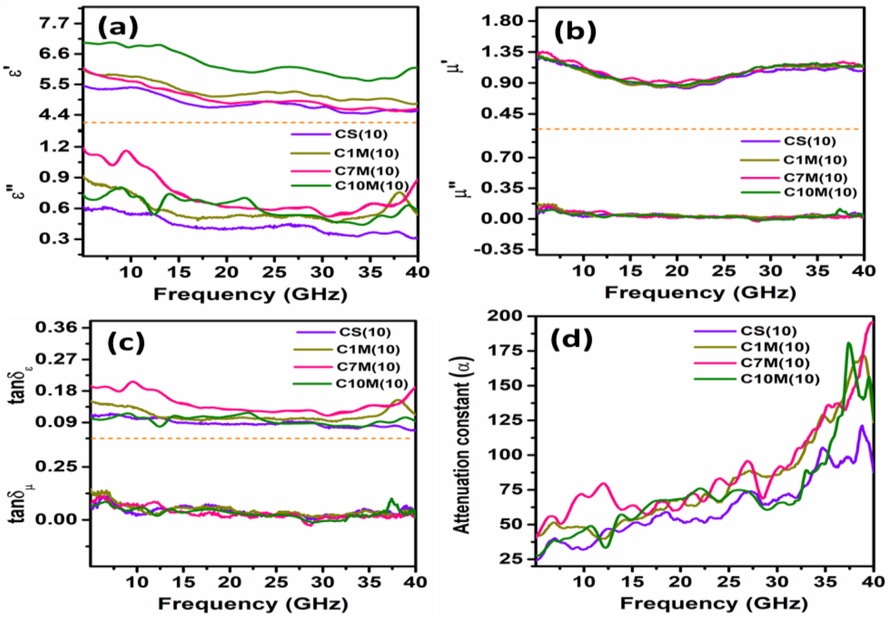

Fig. 5 (a) complex permittivity (b) complex permeability (c) dielectric and magnetic loss tangents and (d) attenuation constants of CS(10), C1M(10), C7M(10) and C10M(10).

Fig. 5 shows the complex permittivity, permeability, dielectric and magnetic loss tangents, and attenuation constant of the composites. The CS(10) composite exhibited a higher real permittivity compared to the other composites, while the real permeability of all the composites is in the same range. The dielectric loss of the C7M(10) composite is slightly higher than that of the rest of the composites, while the magnetic loss results from all the composites were similar. A comparable attenuation constant to that of C40 was observed for all the composites, with the CS(10) composite exhibiting the least attenuation constant.

For the C7M(20) composite, the minimum RL observed are -22.4 and -40.1 dB resulting at 25.9 and 21.7 GHz for 2.5 and 3.0 mm thickness, while for the C10M(20) composite, the RL is -27.4 dB at 22.6 GHz for 2.5 mm and -39.7 dB at 18.2 GHz for 3 mm. The electromagnetic parameters of the composites are shown in Fig. 6. The magnetic properties are almost similar in all composites and are comparable to that of 10 wt% of Magnetite composites. However, the dielectric properties of the composites exhibited an increase from that of the composites with 10 wt% of Magnetite, which in turn resulted in a comparatively better attenuation constant.

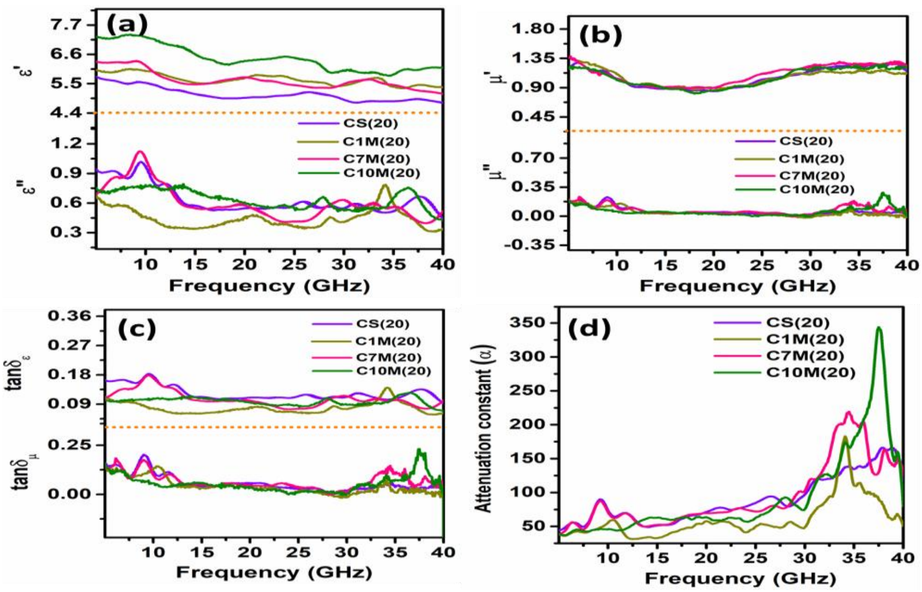

Fig. 5.15 (a) complex permittivity (b) complex permeability (c) dielectric and magnetic loss tangents and (d) attenuation constants of CS(20), C1M(20), C7M(20) and C10M(20).

Table 5.3 RL, minimum reflection frequency (fm), and EABW of the composites

Composites	Thickness: 3.0 mm			Thickness: 2.5 mm		
	RL (dB)	fm (GHz)	EABW (GHz)	RL (dB)	fm (GHz)	EABW (GHz)
C20	-22.7	21.3	5.8	-38.1	27.6	11.1
C30	-18.7 -16.7	18.5 33.9	3.7 4.8	-27.1	23.0	5.1
C40	-14.5	16.8	3.2	-15.3	19.9	5.5
CS(10)	-30.5	20.6	5.4	-25.4	25.8	8.6
C1M(10)	-40.0	21.3	5.5	-35.4	25.9	6.7
C7M(10)	-42.8	20.4	5.8	-31.4	25.4	7.3
C10M(10)	-37.6	20.3	4.3	-29.8	23.4	5.3
CS(20)	-30.0	20.9	6.0	-30.5	26.0	6.9
C1M(20)	-46.0	19.2	4.0	-44.6	23.1	4.9
C7M(20)	-40.0	21.6	5.5	-22.3	25.8	9.4
C10M(20)	-39.6	18.1	3.9	-27.3	22.5	4.6

Table 5.3 compares the results of microwave absorption properties resulting from all the C12A7:e-@G/Magnetite/wax composites. The better microwave attenuation properties of C12A7:e-@G/Magnetite composites resulted from the individual contributions from the highly conducting C12A7:e-@G, magnetic Magnetite NPs, and their synergy. The high electrical conductivity of C12A7:e-@G arises from the cage-trapped electron anions and highly graphitized carbon interface. Even though the attenuation due to dipolar polarizations possible from the functional groups is negligible in C12A7:e-@G, additional enhancement is possible due to the increased conductivity resulting from the high graphitization degree of the carbon envelope. Moreover, the high-frequency EM responses are also possible from C12A7:e-@G due to the electron anions. Further, a significant effect of the MWS effect also contributes to microwave attenuation due to the various interfaces present in the material.

In this case, the magnetic nanoparticles have a considerable impact on the impedance matching as well as microwave absorption properties of the composites. It is the numerous magnetic losses and the interface effect that are introduced by the magnetic particle that are responsible for the majority of the contribution in this case. The domain wall resonance and spin resonance are the two fundamental phenomena that are responsible for the magnetic loss that occurs in the material. Generally speaking, domain wall resonance takes place at lower frequencies, and the magnetic losses that occur in the microwave frequency band are caused by natural resonance, exchange resonance, and eddy current loss (Shukla, 2019; Zhao et al., 2017). However, the 7M and 10M particles will have Eddy current losses due to their unique flake-like and polyhedron-like morphology, which will provide sufficient area to induce Eddy voltage (Shukla, 2019). This is despite the fact that the Eddy current loss that is caused by Magnetite NPs will be relatively low in comparison to that of the bulk particles. An additional factor that significantly adds to the magnetic losses that are linked with magnetite nanoparticles is the magnetic anisotropy that is caused by the anisotropic morphology. Particularly, the anisotropic effect has a substantial consequence in nanomaterials because it causes the breakage of some exchange bonds, which in turn will further influence the relaxation duration and frequency (Liang et al., 2020; Liang, et al., 2015). However, this is not the only occurrence of this impact. Pan et al. studied the dependence of shape anisotropy of Magnetite NPs and demonstrated that higher electrical conductivity, better anti-reflection surfaces, and multiple scattering are closely related to the anisotropic cross- linked structures of Magnetite NPs (Pan et al., 2020). According to Liang et al. (2015), the magnetic anisotropy that is caused by the morphology can cause the permeability to become wider, and it can also cause the scattering of electromagnetic radiation to become more intense, which ultimately results in an increase in the microwave absorption. In this research, Liang and colleagues investigated the form anisotropy of superparamagnetic magnetite nanoparticles (NPs) with a variety of morphologies, including hexagonal-like, rod-like, triangle-like, and quadrilateral-like morphologies. The quadrilateral-like nanoparticles were the ones that displayed the highest specific absorption rate (SAR) among all of them, and as a result, they were able to transform the microwave energy into heat energy (Liang et al., 2020).

Conclusion

The nature of the carbon interface and the electrical conductivity has been modified by simply modifying the synthesis conditions. The mayenite electride with graphitic carbon interface (C12A7:e-@G) exhibited high attenuation potential due to its unique structural and morphology derived properties. The impedance matching and microwave absorption of C12A7:e-@G are further improved by incorporating four types of Magnetite nanoparticles having various sizes and morphology. All the composites exhibit promising properties to act as potential candidates for microwave absorption applications owing to the high conductivity, suitable magnetic properties, and synergy among the materials. The tuned electromagnetic parameters arising from high electrical conductivity and effective polarization at different interfaces, as well as the magnetic losses from Magnetite contribute to the exceptional microwave attenuation preparties of the material. Among the composites, the C12A7:e-@G/Magnetite composite with sphere-like morphology exhibited better impedance matching resulting in a minimum RL of -46.0 dB at 19.2 GHz with an EABW of 4.0 GHz for a thickness of 3 mm, which is ascribed to the smaller size of the nanoparticles having a maximum surface area facilitating interfacial and dipolar polarization. This study demonstrated the potential of C12A7:e-@G/Magnetite composite, which can act as an alternative for the high-cost carbon nanostructures-derived EM absorbers for high-frequency applications. Moreover, this ceramic material-based system can be further studied for widening the application possibilities to the harsh-environmental conditions.

References

[1] Anand, S., & Pauline, S. (2021). Effective lightweight, flexible and ultrathin PVDF/rGO/ $Ba_2Co_2Fe_{12}O_{22}$ composite films for electromagnetic interference shielding applicatio ns. *Nanotechnology*, *32*(47) *475707.* https://doi.org/10.1088/1361-6528/ABED75

[2] Anand, S., Pauline, S., & Prabagar, C. J. (2020). Zr doped Barium hexaferrite nanoplatelets and RGO fillers embedded Polyvinylidenefluoride composite films for electromagnetic interference shielding applications. *Polymer Testing*, *86*. *106504* https://doi.org/10.1016/j.polymertesting.2020.106504

[3] Andrade, R. G. D., Veloso, S. R. S., & Castanheira, E. M. S. (2020). Shape Anisotropic Iron Oxide-Based Magnetic Nanoparticles: Synthesis and Biomedical Applications. *International Journal of Molecular Sciences, 21*(7), 2455. https://doi.org/10.3390/ijms21072455

[4] Badreldin, A., Abusrafa, A. E., & Abdel-Wahab, A. (2020). Oxygen-deficient perovskites for oxygen evolution reaction in alkaline media: a review. *Emergent Materials*, *3*(5), 567–590. https://doi.org/10.1007/S42247-020-00123-Z/FIGURES/12

[5] Batool, S. S., Imran, Z., Rasool, K., Ambreen, J., Hassan, S., Arif, S., Ahmad, M., & Rafiq, M. A. (2020). Study of electric conduction mechanisms in bismuth silicate nanofibers. *Scientific Reports*, *10*(1), 1–10. https://doi.org/10.1038/s41598-020-59563-6

[6] Cai, M., Yan, H., Li, Y., -, al, Duan, Z., Jiang, Y., Tai -, H., Wang, L., He, Y., Liu, D., Zhang, J., Xue, W., & Chen, X.-Y. (2020). $Ti_3C_2T_x$ MXenes as thin broadband absorbers. *Nanotechnology*, *31*(27), 275301. https://doi.org/10.1088/1361- 6528/AB80FD

[7] Cheng, H., Lu, Z., Gao, Q., Zuo, Y., Liu, X., Guo, Z., Liu, C., & Shen, C. (2021). PVDF-Ni/PE-CNTs Composite Foams with Co-Continuous Structure for Electromagnetic Interference Shielding and Photo-Electro-Thermal Properties. *Engineered Science*, *16*, 331–340. https://doi.org/10.30919/ES8D518

[8] Cheng, H., Pan, Y., Chen, Q., Che, R., Zheng, G., Liu, C., Shen, C., & Liu, X. (2021). Ultrathin flexible poly(vinylidene fluoride)/MXene/silver nanowire film with outstanding specific EMI shielding and high heat dissipation. *Advanced Composites and Hybrid Materials*, *4*(3), 505–513. https://doi.org/10.1007/S42114-021-00224-1

[9] CHOFORM 5528 Ag/Cu Moisture Cure One Component Form-In-Place Silicone EMI Gasketing | ParkerGB. Retrieved February 20, 2022, from https://ph.parker.com/gb/en/choform-5528-robotically-dispensed-form-in-place-emi-gasketing/19-26-5528-0850

[10] Fatima, H., Lee, D. W., Yun, H. J., & Kim, K. S. (2018). Shape-controlled synthesis of magnetic Fe_3O_4 nanoparticles with different iron precursors and capping agents. *RSC Advances*, *8*(41), 22917–22923. https://doi.org/10.1039/C8RA02909A

[11] *Global Market For Emi/Rfi Shielding To Reach Nearly $6 Billion In 2018*. Retrieved February 20, 2022, from https://www.bccresearch.com/pressroom/pls/global-market- emi-rfi-shielding-reach-nearly-$6-billion-2018

[12] Goel, S., Tyagi, A., Garg, A., Kumar, S., Baskey, H. B., Gupta, R. K., & Tyagi, S. (2021). Microwave absorption study of composites based on CQD@$BaTiO_3$ core shell and $BaFe_{12}O_{19}$ nanoparticles. *Journal of Alloys and Compounds*, *855*. https://doi.org/10.1016/J.JALLCOM.2020.157411

[13] Jiao, S., Wu, M., Yu, X., & Zhang, H. (2020). Enhanced Microwave Absorption: The Composite of Fe_3O_4 Flakes and Reduced Graphene Oxide with Improved Interfacial Polarization. *Advanced Engineering Materials*, *22*(4), 1901299. https://doi.org/10.1002/ADEM.201901299

[14] Jin, L., Wang, J., Wu, F., Yin, Y., & Zhang, B. (2021). MXene@Fe_3O_4 microspheres/fibers composite microwave absorbing materials: Optimum composition and performance evaluation. *Carbon*, *182*, 770–780. https://doi.org/10.1016/J.CARBON.2021.06.073

[15] Kazmi, S. J., Nadeem, M., Warsi, M. A., Manzoor, S., Shabbir, B., & Hussain, S. (2022). PVDF/CFO-anchored CNTs ternary composite system with enhanced EMI shielding and EMW absorption properties. *Journal of Alloys and Compounds*, *903*, 163938. https://doi.org/10.1016/J.JALLCOM.2022.163938

[16] Kondawar, S. B., & Modak, P. R. (2020). "Theory of EMI shielding" *Materials for Potential EMI Shielding Applications* 9–25. Elsevier. https://doi.org/10.1016/b978-0- 12-817590-3.00002-6

[17] Koo, C., Hong, H., Im, P. W., Kim, H., Lee, C., Jin, X., Yan, B., Lee, W., Im, H. J., Paek, S. H., & Piao, Y. (2020). Magnetic and near-infrared derived heating characteristics of dimercaptosuccinic acid coated uniform Fe@Fe_3O_4 core–shell nanoparticles. *Nano Convergence*, *7*(1), 1–9. https://doi.org/10.1186/S40580-020-00229-4/FIGURES/6

[18] Kruželák, J., Kvasničáková, A., Hložeková, K., & Hudec, I. (2021). Progress in polymers and polymer composites used as efficient materials for EMI shielding. *Nanoscale Advances*, *3*(1), 123–172. https://doi.org/10.1039/D0NA00760A

[19] Li, Yang, Qing, Y., Zhao, B., Bai, P., Zhang, R., Yao, H., & Luo, F. (2021). Tunable magnetic coupling and dipole polarization of core-shell Magnéli Ti_4O_7 ceramic/magnetic metal possessing broadband microwave absorption properties. *Ceramics International*, *47*(23), 33373–33381. https://doi.org/10.1016/J.CERAMINT.2021.08.240

[20] Li, Ye, Li, S., Zhang, T., Shi, L., Liu, S., & Zhao, Y. (2019). 3D hierarchical Co_3O_4/Reduced graphene oxide/melamine derived carbon foam as a comprehensive microwave absorbing material. *Journal of Alloys and Compounds*, *792*, 424–431. https://doi.org/10.1016/j.jallcom.2019.03.359

[21] Ma, J., Shu, J., Cao, W., Zhang, M., Wang, X., Yuan, J., & Cao, M. (2019). A green fabrication and variable temperature electromagnetic properties for thermal stable microwave absorption towards flower-like Co_3O_4@rGO/SiO_2 composites. *Composites Part B: Engineering*, *166*, 187–195. https://doi.org/10.1016/j.compositesb.2018.11.119

[22] Ma, Y., Quan, B., Zeng, Z., Zhang, Y., Zhang, L., Wang, Y., & Huang, X. (2021). Multiple interface-induced evolution of electromagnetic patterns for efficient microwave absorption at low thickness. *Inorganic Chemistry Frontiers*, *8*(7), 1810–1818. https://doi.org/10.1039/d0qi01486a

[23] Nazir, A. (2020). A review of polyvinylidene fluoride (PVDF), polyurethane (PU), and polyaniline (PANI) composites-based materials for electromagnetic interference shielding:. 0892705720925120. https://doi.org/10.1177/0892705720925120

[24] Pan, J., Guo, H., Wang, M., Yang, H., Hu, H., Liu, P., & Zhu, H. (2020). Shape anisotropic Fe_3O_4 nanotubes for efficient microwave absorption. *Nano Research*, *13*(3), 621–629. https://doi.org/10.1007/S12274-020-2656-5

[25] Pang, W., Xue, J., & Pang, H. (2019). A High Energy Density Azobenzene/Graphene Oxide Hybrid with Weak Nonbonding Interactions for Solar Thermal Storage. *Scientific Reports*, *9*(1), 1–12. https://doi.org/10.1038/s41598-019-41563-w

[26] *Parker Chomerics CHO-FORM 5532 EMI*

Shielding Material datasheet. Retrieved February 20, 2022, from http://www.lookpolymers.com/polymer_Parker-Chomerics- CHO-FORM-5532-EMI-Shielding-Material.php

[27] Qi, Q., Ma, L., Zhao, B., Wang, S., Liu, X., Lei, Y., & Park, C. B. (2020). An Effective Design Strategy for the Sandwich Structure of PVDF/GNP-Ni-CNT Composites with Remarkable Electromagnetic Interference Shielding Effectiveness. *ACS Applied Materials and Interfaces*, *12*(32), 36568–36577. https://doi.org/10.1021/acsami.0c10600

[28] Rajavel, K., Luo, S., Wan, Y., Yu, X., Hu, Y., Zhu, P., Sun, R., & Wong, C. (2020). 2D $Ti_3C_2T_x$ MXene/polyvinylidene fluoride (PVDF) nanocomposites for attenuation of electromagnetic radiation with excellent heat dissipation. *Composites Part A: Applied Science and Manufacturing*, *129*, 105693. https://doi.org/10.1016/J.COMPOSITESA.2019.105693

[29] Rudradawong, C., Kitiwan, M., Goto, T., & Ruttanapun, C. (2020). Positive ionic conduction of mayenite cement $Ca_{12}Al_{14}O_{33}$/nano-carbon black composites on dielectric and thermoelectric properties. *Materials Today Communications*, *22*, 100820. https://doi.org/10.1016/j.mtcomm.2019.100820

[30] Shayesteh Zeraati, A., Mende Anjaneyalu, A., Pawar, S. P., Abouelmagd, A., & Sundararaj, U. (2021). Effect of secondary filler properties and geometry on the electrical, dielectric, and electromagnetic interference shielding properties of carbon nanotubes/polyvinylidene fluoride nanocomposites. *Polymer Engineering & Science*, *61*(4), 959–970. https://doi.org/10.1002/PEN.25591

[31] Shu, R., Li, X., Tian, K., & Shi, J. (2022). Fabrication of bimetallic metal-organic frameworks derived Fe_3O_4/C decorated graphene composites as high-efficiency and broadband microwave absorbers. *Composites Part B: Engineering*, *228*, 109423. https://doi.org/10.1016/J.COMPOSITESB.2021.109423

[32] Soares, B. G., Barra, G. M. O., & Indrusiak, T. (2021). Conducting polymeric composites based on intrinsically conducting polymers as electromagnetic interference shielding/microwave absorbing materials—a review. *Journal of Composites Science*, *5*(7), 173. https://doi.org/10.3390/JCS5070173

[33] Srivastava, S. K., & Manna, K. (2022). Recent Advancements in Electromagnetic Interference Shielding Performance of Nanostructured Materials and their Nanocomposites: A Review. *Journal of Materials Chemistry A*, *6*, 4883–5230. https://doi.org/10.1039/D1TA09522F

[34] Sushmita, K., Formanek, P., Krause, B., Pötschke, P., & Bose, S. (2022). Distribution of Carbon Nanotubes in Polycarbonate-Based Blends for Electromagnetic Interference Shielding. *ACS Applied Nano Materials*, *5*(1), 662–677. https://doi.org/10.1021/acsanm.1c03442

[35] Wanasinghe, D., Aslani, F., Ma, G., & Habibi, D. (2020). Advancements in electromagnetic interference shielding cementitious composites. In *Construction and Building Materials*, 231, 117116. https://doi.org/10.1016/j.conbuildmat.2019.117116

[36] Wang, C., Ma, Y., Qin, Z., Wang, J., & Zhong, B. (2021). Synthesis of hollow spherical MoS_2@Fe_3O_4-GNs ternary composites with enhanced microwave absorption performance. *Applied Surface Science*, *569*, 150812. https://doi.org/10.1016/J.APSUSC.2021.150812

[37] Wang, X., Huang, J., Feng, H., Li, J., Pu, Z., & Yin, X. (2021). Facile preparation of the dendritic Fe_3O_4 with a core-shell microstructure in SiO_2-B_2O_3-Al_2O_3-CaO-Fe_2O_3 glass-ceramic system for enhanced microwave absorbing performance. *Journal of Alloys and Compounds*, *877*, 160147. https://doi.org/10.1016/J.JALLCOM.2021.160147

[38] Wang, X. X., Ma, T., Shu, J. C., & Cao, M. S. (2018). Confinedly tailoring Fe_3O_4 clusters-NG to tune electromagnetic parameters and microwave absorption with broadened bandwidth. *Chemical Engineering Journal*, *332*, 321–330. https://doi.org/10.1016/j.cej.2017.09.101

[39] Wang, Yan, Gao, X., Lin, C., Shi, L., Li, X., & Wu, G. (2019). Metal organic frameworks-derived Fe-Co nanoporous carbon/graphene composite as a high- electromagnetic performance wave absorber. *Journal of Alloys and Compounds*, *785*, 765–773. https://doi.org/10.1016/J.JALLCOM.2019.01.271

[40] Wei, H., Cheng, L., & Shchukin, D. (2020). Effect of porous structure on the microwave absorption capacity of soft magnetic connecting network Ni/Al_2O_3/Ni film. *Materials*, *13*(7), 1764. https://doi.org/10.3390/MA13071764

[41] Wu, W. W., Liu, Y., Zhou, Q., Liu, L. N., Chen, X. M., & Liu, P. (2020). Microwave absorbing properties of FeB/B_4C nanowire composite. *Ceramics International*, *46*(3), 4020–4023. https://doi.org/10.1016/J.CERAMINT.2019.10.052

[42] Xu, N., Yan, H., Jiao, X., Jiang, L., Zhang, R.,

Wang, J., Liu, Z., Liu, Z., Gu, Y., Gang, F., Wang, X., Zhao, L., & Sun, X. (2020). Effect of OH− concentration on Fe_3O_4 nanoparticle morphologies supported by first principle calculation. *Journal of Crystal Growth*, *547*. https://doi.org/10.1016/J.JCRYSGRO.2020.125780

[43] Ye, X., Chen, Z., Li, M., Wang, T., Wu, C., Zhang, J., Zhou, Q., Liu, H., & Cui, S. (2020). Hollow SiC foam with a double interconnected network for superior microwave absorption ability. *Journal of Alloys and Compounds*, *817*, 153276. https://doi.org/10.1016/J.JALLCOM.2019.153276

[44] Zeng, G., Li, X., Wei, Y., Guo, T., Huang, X., Chen, X., & Tang, X. Z. (2021). Significantly toughened SiC foams with enhanced microwave absorption via in situ growth of Si_3N_4 nanowires. *Chemical Engineering Journal*, *426*, 131745. https://doi.org/10.1016/J.CEJ.2021.131745

[45] Zeng, X., Zhu, L., Yang, B., & Yu, R. (2020). Necklace-like Fe_3O_4 nanoparticle beads on carbon nanotube threads for microwave absorption and supercapacitors. *Materials and Design*, *189*, 108517. https://doi.org/10.1016/j.matdes.2020.108517

[46] Zhang, D., Zhang, H., Cheng, J., Raza, H., Liu, T., Liu, B., Ba, X., Zheng, G., Chen, G., & Cao, M. (2020). Customizing coaxial stacking VS_2 nanosheets for dual-band microwave absorption with superior performance in the C-And Ku-bands. *Journal of Materials Chemistry C*, *8*(17), 5923–5933. https://doi.org/10.1039/d0tc00763c

[47] Zhang, H., Zhang, G., Gao, Q., Tang, M., Ma, Z., Qin, J., Wang, M., & Kim, J. K. (2020). Multifunctional microcellular PVDF/Ni-chains composite foams with enhanced electromagnetic interference shielding and superior thermal insulation performance. *Chemical Engineering Journal*, *379*. https://doi.org/10.1016/J.CEJ.2019.122304

[48] Zhao, B., Zeng, S., Li, X., Guo, X., Bai, Z., Fan, B., & Zhang, R. (2020). Flexible PVDF/carbon materials/Ni composite films maintaining strong electromagnetic wave shielding under cyclic microwave irradiation. *Journal of Materials Chemistry C*, *8*(2), 500–509. https://doi.org/10.1039/C9TC05462F

[49] Zhou, L., Yan, J., Huang, J., Wang, H., Wang, X., & Wang, Z. (2021). Dielectric and microwave absorption properties of FeSiAl/Al_2O_3 composites containing FeSiAl particles of different sizes. *Ceramics International*, *47*(6), 7831–7836. https://doi.org/10.1016/J.CERAMINT.2020.11.129